COMMUNICATION

$^{13}C^{\alpha}$ decoupling during direct observation of carbonyl resonances in solution NMR of isotopically enriched proteins

Jinfa Ying · Fang Li · Jung Ho Lee · Ad Bax

Abstract Direct detection of ^{13}C can be advantageous when studying uniformly enriched proteins, in particular for paramagnetic proteins or when hydrogen exchange with solvent is fast. A scheme recently introduced for long-observation-window band-selective homonuclear decoupling in solid state NMR, LOW-BASHD (Struppe et al. in J Magn Reson 236:89–94, 2013) is shown to be effective for $^{13}C^{\alpha}$ decoupling during direct $^{13}C'$ observation in solution NMR experiments too. For this purpose, adjustment of the decoupling pulse parameters and delays is demonstrated to be important for increasing spectral resolution, to reduce three-spin effects, and to decrease the intensity of decoupling side-bands. LOW-BASHD then yields $^{13}C'$ line widths comparable to those obtained with the popular IPAP method, while enhancing sensitivity by ca 35 %. As a practical application of LOW-BASHD decoupling, requiring quantitative intensity measurement over a wide dynamic range, the impact of lipid binding on the $^{13}C'$-detected NCO spectrum of the intrinsically disordered protein α-synuclein is compared with that on the ^1H-detected ^1H–^{15}N HSQC spectrum. Results confirm that synuclein's "dark state" behavior is not caused by paramagnetic relaxation or rapid hydrogen exchange.

J. Ying · F. Li · J. H. Lee · A. Bax (✉)
Laboratory of Chemical Physics, National Institute of Diabetes and Digestive and Kidney Diseases, National Institutes of Health, Bethesda, MD 20892, USA
e-mail: bax@nih.gov

Heteronuclear broad-band decoupling of scalar spin–spin interactions is a standard and widely used method for enhancing resolution and sensitivity in both solution and solid-state NMR experiments. Removal of homonuclear couplings is technically more challenging because manipulation of a given spin by radiofrequency (RF) irradiation prohibits simultaneous detection of the nearby resonating coupling partner. Although such J splittings can be removed by non-linear data processing, such as the maximum entropy method (Delsuc and Levy 1988), this approach is not widely used. Until relatively recently, broad-band homonuclear decoupling of scalar interactions was largely restricted to the indirectly detected dimensions of multi-dimensional NMR experiments, where constant-time evolution and BIRD methods have been widely used for this purpose (Bax et al. 1979; Bax and Freeman 1981; Garbow et al. 1982; Bax 1983; van de Ven and Philippens 1992; Vuister and Bax 1992). Although the BIRD mode of homonuclear decoupling was initially designed for use during direct signal observation (Garbow et al. 1982), the requirement for multiple relatively lengthy time gaps during the FID made it ill suited for rapidly relaxing systems such as proteins.

Homonuclear splittings in the directly detected dimension can also be removed by spin-state selective techniques, where one of the components of a doublet is observed at enhanced intensity while the other one is suppressed (Meissner et al. 1997; Bermel et al. 2005), and this approach is widely used to enhance sensitivity and

resolution of ^{13}C-detected experiments on isotopically enriched proteins (Felli and Pierattelli 2014). Alternatively, band-selective decoupling has been used for this purpose, either using shaped or adiabatic pulses, both for ^{13}C–^{13}C and ^{1}H–^{1}H decoupling (McCoy and Mueller 1992b; Hammarström and Otting 1994; Vander Kooi et al. 1999; Bermel et al. 2003; Vogeli et al. 2005). Challenges with these methods relate to relatively large Bloch–Siegert shifts, the need to position the side-bands associated with the homonuclear RF gating process outside of the spectral region of interest, and the significant loss in the duty cycle available for actual signal observation. More recently, elegant and effective methods have been introduced which provide broad-band ^{1}H and, at least in principle, ^{13}C decoupling by periodically interrupting the FID by combinations of selective and non-selective RF pulses in the presence of pulsed field gradients (Zangger and Sterk 1997; Nilsson and Morris 2007; Meyer and Zangger 2013; Sakhaii et al. 2013). When applied in a broad-band manner, this decoupling mode restricts itself to a small volume fraction of the total sample, reducing sensitivity. However, when implemented in a band-selective manner, such pulse-interrupted free precession methods can actually enhance sensitivity and resolution of experiments that rely on ^{1}H^{N} detection in peptides and proteins (Ying et al. 2014).

With the introduction of new probe technology that optimizes ^{13}C-detected experiments, direct ^{13}C observation has gained considerable popularity for studying proteins. Reduced impact from paramagnetic broadening, absence of solvent suppression problems, and the ability to study proteins over a wide range of physiological relevant conditions, unhampered by rapid hydrogen exchange, have boosted the use of this technology (Bermel et al. 2003, 2006, 2012; Eletsky et al. 2003; Gil et al. 2013). Although initially such experiments often used adiabatic homonuclear decoupling, for reasons listed above these subsequently have been modified to rely on spin-state-selective excitation (SSE) or in-phase/antiphase (IPAP) methods (Meissner et al. 1997; Bermel et al. 2005; Barbet-Massin et al. 2013).

Here, we demonstrate that the so-called long-observation-window band-selective homonuclear decoupling method, or LOW-BASHD, recently introduced for solid-state NMR experiments (Struppe et al. 2013), can be readily adapted for solution measurements. LOW-BASHD offers advantages over IPAP and SSE in terms of sensitivity and a twofold reduction in the minimum number of phase cycling steps needed.

The often narrower line widths observed in solution compared to solid state NMR pose additional challenges, however. In particular, residual splittings in decoupled spectra that result from the so-called 3-spin effect (Barker et al. 1985; Shaka et al. 1987) can become quite pronounced if decoupling parameters are not optimized. Also,
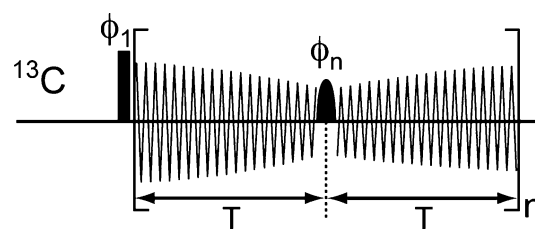

Fig. 1 Schematic depiction of the pulse-interrupted FID during LOW-BASHD decoupling of the ^{13}C′ FID. The ^{13}C$^{\alpha}$ 180° pulses are applied with the carrier at the ^{13}C′ frequency, with the shape of the center lobe of a sinc function of duration 22,600/ν_C μs, where ν_C is the ^{13}C frequency in MHz, and amplitude modulated by a cosine function at a frequency of $\delta \times \nu_C$, where δ is the offset in ppm ($\delta \approx 118$) of the ^{13}C′ carrier relative to 59 ppm ^{13}C$^{\alpha}$ frequency. The pulse spacing, 2T, is 5 ms. The RF phases ϕ_n of the decoupling pulses follow the MLEV16 pattern: AABB BAAB BBAA ABBA, where A = 180$_x$ and B = 180$_{-x}$. A 2-step phase cycle (ϕ_1 = x, −x; Receiver x, −x) is needed to eliminate ringing effects induced by the ϕ_n pulses or, alternatively, the "dead time" following the ϕ_n pulses must be extended to ≥*ca* 13 μs. Bruker pulse sequence code is included as Supplementary Material

we find that relatively close spacing between 180° decoupling pulses is needed to avoid strong decoupling modulation side bands, and that a phase alternation scheme similar to that used for the MLEV16 heteronuclear decoupling schemes (Levitt et al. 1982) is important to improve decoupling and reduce artifacts. We demonstrate that effective ^{13}C$^{\alpha}$ decoupling during ^{13}C′ detection is readily feasible over a range of static magnetic field strengths, both for a small folded protein (GB3) and for an intrinsically disordered protein (α-synuclein).

The implementation of LOW-BASHD on a modern NMR spectrometer has been described previously (Struppe et al. 2013). Effectively, a series of 180° ^{13}C$^{\alpha}$ pulses, spaced by intervals 2T, is applied during detection of the ^{13}C′ FID (Fig. 1), with the first such pulse being applied at time T after the ^{13}C′ observe pulse. Using a digital receiver unit, with rapid oversampling of the FID, the receiver unit is blanked for the duration of the ^{13}C$^{\alpha}$ pulse plus a short (5 μs) recovery period, which generally amounts to a fraction of the dwell time (reciprocal of the ^{13}C′ spectral window) used and causes attenuation of the corresponding datapoint. Although in principle the attenuated data-points can be rescaled or otherwise corrected to reduce resulting sidebands in the Fourier transformed spectrum (Struppe et al. 2013), we find that this generally is not necessary unless dealing with spectra that have a very high dynamic range.

For ideal ^{13}C$^{\alpha}$ inversion pulses, due to ^{1}J$_{C′C\alpha}$ dephasing the ^{13}C′ FID will be attenuated by a factor cos(π^{1}J$_{C′C\alpha}$T) just prior and following these 180° ^{13}C$^{\alpha}$ pulses. With ^{1}J$_{C′C\alpha}$ ≈ 53 Hz, an interpulse spacing of 2T ≤ 5 ms suffices to
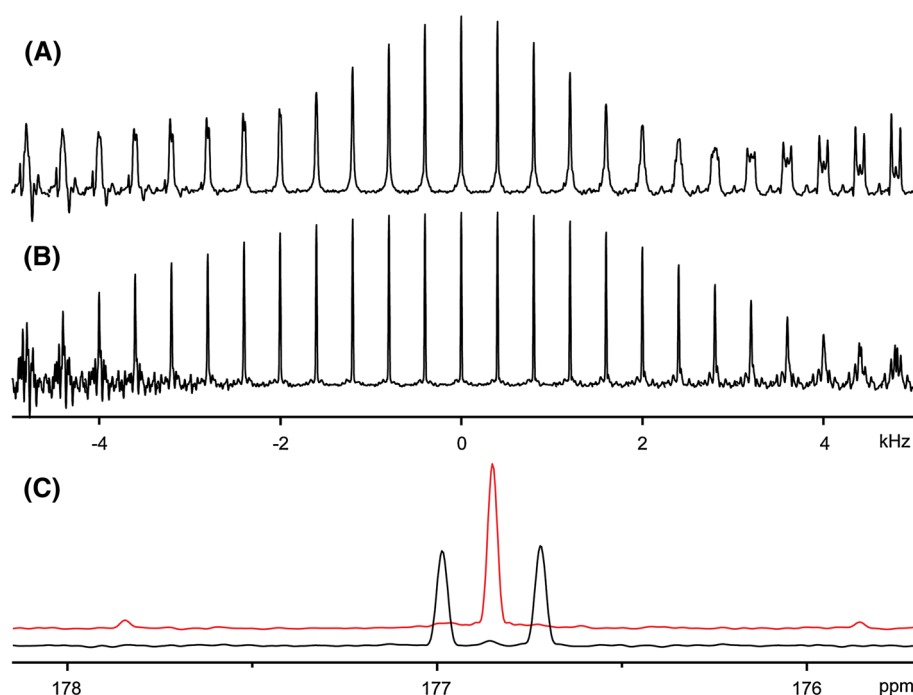
Fig. 2 Offset dependence of LOW-BASHD decoupling performance for a sample of U–^{13}C valine, observing ^{13}C′ with ^{13}C$^\alpha$ decoupling applied at offsets relative to ^{13}C$^\alpha$ (59 ppm) ranging from −4.8 to +4.8 kHz, in increments of 1.99 ppm (400 Hz). Spectra have been recorded at 201 MHz ^{13}C frequency, using $2T = 5$ ms, and sinc-shaped 180° pulses of 113 μs duration. The duration of the acquisition time was 200 ms, and data were apodized with a squared 90°-shifted sine bell window prior to zero filling and Fourier transformation. **A** For constant ^{13}C phase ($\phi_n = x$), and **B** in the presence of MLEV16 phase alternation. **C** Comparison of the LOW-BASHD ^{13}C′ spectrum (*red*) with the ^{13}C$^\alpha$-coupled spectrum, each recorded with two transients. Weak decoupling sidebands in the LOW-BASHD spectrum are seen at offsets of ±200 Hz relative to the main peak

keep small the resulting amplitude modulation sidebands after Fourier transformation, which are spaced at integral multiples of $(2T)^{-1}$ relative to the main resonance, with the first set being by far the strongest.

The effective magnetic field strength in the rotating frame, experienced by a ^{13}C′ spin during application of the ^{13}C$^\alpha$ pulses, corresponds to the vector sum of the ^{13}C$^\alpha$ RF field and the ^{13}C′ offset frequency in the ^{13}C$^\alpha$ rotating frame. This off-resonance effect, commonly referred to as a Bloch–Siegert shift of the second kind (Cavanagh et al. 2007), moves the effective resonance frequency away from that of the applied RF field. To first order, this effect can be eliminated by simultaneously applying a second, equally strong RF field at an offset frequency opposite to that of ^{13}C$^\alpha$, i.e., at about 300 ppm. In practice, this is done by cosine modulation of a 180° ^{13}C′ pulse at the frequency difference between ^{13}C′ and ^{13}C$^\alpha$ of a pulse applied at the ^{13}C′ carrier (McCoy and Mueller 1992a). Some fine-tuning of this frequency difference, effectively moving the ^{13}C$^\alpha$ carrier to ca 59 ppm, is needed to simultaneously reduce the three-spin effect (see below) for all different residue types. We find that decoupling pulses corresponding to (prior to cosinusoidal amplitude modulation) the center lobe of a sinc function are suitable for this purpose, with

the duration of the sinc-shaped pulse set to $22{,}600/\nu_C$, where ν_C is the ^{13}C frequency in Hz. The pulse shape and its duration were selected by trial and error, after evaluating a range of different selective pulses and pulse combinations, prior to becoming aware of the earlier solid-state LOW-BASHD work (Struppe et al. 2013). The fact that our parameters independently resulted in a shape and duration rather similar to those used in the solid state study suggests that no large further improvement is attainable for the parameters of this pulse scheme. However, as previously noted for the band-selective ^{1}H$^\alpha$ decoupling in ^{1}H^N-detected experiments (Ying et al. 2014), and can be seen from comparison of Fig. 2A, B, altering the phases of the ^{13}C$^\alpha$ decoupling pulses following the recipe of the MLEV16 scheme (see caption to Fig. 1), is critical for good performance.

The decoupling bandwidth performance of the LOW-BASHD decoupling scheme is demonstrated for a sample of uniformly ^{13}C-enriched valine. The center of the ^{13}C$^\alpha$ RF field is varied stepwise from 83 to 35 ppm by changing the frequency of the cosine amplitude modulation of the decoupling pulses from 18.9 to 28.5 kHz (at 201 MHz ^{13}C frequency), while keeping all other parameters constant. As can be seen in Fig. 2B, the decoupling bandwidth exceeds
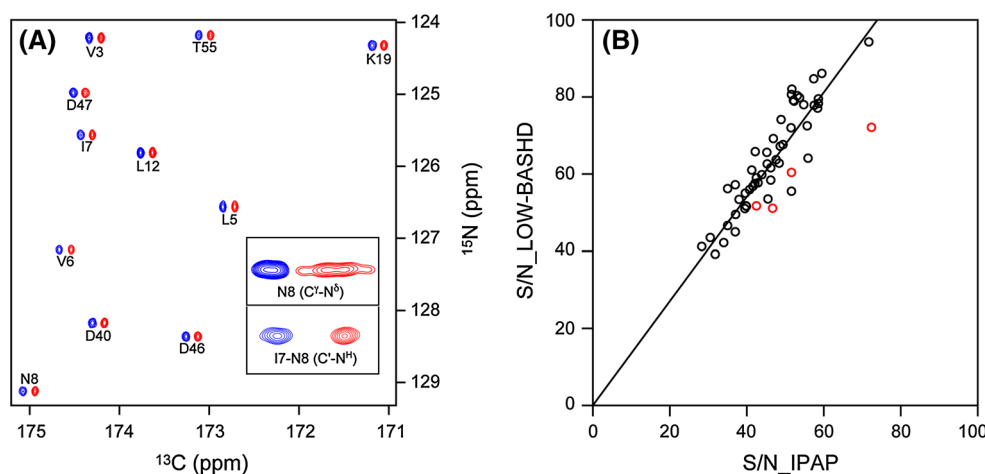
Fig. 3 Comparison of LOW-BASHD and IPAP 2D NCO spectra. **A** Expanded region of the LOW-BASHD NCO spectrum (*red contours*) of a sample of uniformly $^{13}C/^{15}N$-enriched GB3, superimposed on the IPAP-NCO spectrum (*blue contours*). Sample conditions: 1.0 mM $^{13}C/^{15}N$-GB3 in 300 μL 20 mM sodium phosphate buffer, 50 mM NaCl, pH 6.2, 5 % D_2O, 293 K, Shigemi microcell. The spectra were recorded on a Bruker Avance-800 spectrometer, equipped with a TCI cryogenically cooled probe, using the pulse sequence presented in the Supplementary Information, and processed with NMRPipe (Delaglio et al. 1995). *Insets* show the poorly decoupled $^{13}C^\gamma$–$^{15}N^\delta$ sidechain correlation of Asn[8], and the well-decoupled C′–N correlation for Ile[7]–Asn[8], where the IPAP spectrum is weaker due to additional long range J_{CC} couplings (peaks have been shifted apart by an additional 6 Hz to avoid overlap in the top insert).

The IPAP NCO spectrum corresponds to the downfield component of the $^{13}C'$–$\{^{13}C^\alpha\}$ doublet component from which the oppositely signed upfield doublet component has been subtracted, after downfield shifting that spectrum by 53 Hz (Bermel et al. 2006). **B** Comparison of S/N in IPAP and LOW-BASHD 2D NCO spectra. Correlations to Gly $^{13}C'$ are shown in *red*. Both data sets were recorded using identical measurement times (~6 h), with 16 FIDs per complex t_1 increment (8 FIDs for the in-phase and 8 FIDS for the antiphase component for the IPAP-CON spectrum; with the spectra shifted and co-added post-processing). As expected, the noise level of the combined IPAP spectrum is 1.4 times higher compared to the LOW-BASHD 2D NCO spectrum. The solid line corresponds to $y = 1.35x$. See Fig. S1 for details of the LOW-BASHD-NCO acquisition parameters

20 ppm, sufficient to cover the entire $^{13}C^\alpha$ region with the exception of Gly. For Gly, which lacks a $^{13}C^\beta$, there is no 3-spin effect and effective decoupling extends over a significantly wider range (ca±15 ppm), and they remain reasonably well decoupled from $^{13}C'$ when using the parameters of Fig. 1. Resonances of Glu/Gln-$^{13}C^\gamma$ and Asp/Asn-$^{13}C^\beta$ resonate outside of the range covered by LOW-BASHD, and therefore are not well decoupled from the sidechain carboxyl nucleus (see inset in Fig. 3A).

Without apodization of the FID, the Val $^{13}C'$ line width obtained with LOW-BASHD decoupling is about 5 Hz, which is comparable to or slightly narrower than those of the individual $^{13}C'$–$\{^{13}C^\alpha\}$ doublet components (Fig. 2C and inset Fig. 3A). Narrower line width in the LOW-BASHD spectrum can result from the partial decoupling of the long-range J_{CC} interactions between the backbone $^{13}C'$ and the sidechain ^{13}C nuclei, sometimes more than off-setting the loss of intensity associated with both imperfect decoupling and the partial $^1J_{C'C\alpha}$ dephasing during the FID.

Figure 3 compares the LOW-BASHD $^{13}C'$-detected NCO spectrum of GB3 with that of the IPAP version of the experiment, confirming that all backbone $^{13}C'$ resonances are properly decoupled from $^{13}C^\alpha$. Weaker and broader, partially decoupled multiplet patterns are seen for the sidechain correlations of several carboxamide moieties of

Asn and Gln residues, exhibiting ^{13}C line widths of ca 15 Hz. Note that, next to the constant $^1J_{C\alpha C'}/2$ difference associated with the IPAP representation, for all correlations there also is a very small change in $^{13}C'$ resonance frequency. A change in frequency in the direction of the $^{13}C'$ carrier results from the second order Bloch–Siegert effect, which is actually doubled in magnitude by the fact that cosine modulation of the decoupling pulses effectively corresponds to two off-resonance RF fields, doubling the offset dependence of the Bloch–Siegert effect of the second kind. The experimentally measured second order Bloch–Siegert effect scales linearly with the $^{13}C'$ offset frequency but is very small (≤±2 Hz) across the entire $^{13}C'$ chemical shift range at 201 MHz, when using the decoupling pulse parameters of the caption to Fig. 1. In practice, we find that the first-order Bloch–Siegert shift of the second kind is not always eliminated completely by the cosine-modulation of the $^{13}C^\alpha$ decoupling pulses, an effect related to the downfield (at ca 300 ppm) sideband falling further from the optimal tuning frequency of the high Q-factor ^{13}C coil and therefore giving rise to a slightly weaker RF field. This first-order Bloch–Siegert shift is constant across the $^{13}C'$ spectrum, and also at most a few Hz.

When observing $^{13}C'$ at a resolution level of ~25 Hz, as can be reached in advanced solid state NMR studies of

polycrystalline proteins, LOW-BASHD decoupling of $^{13}C^\alpha$ is very robust and relatively insensitive to parameter settings (Struppe et al. 2013). However, when aiming for much higher resolution in liquid state NMR, the requirements on decoupling performance become correspondingly more demanding. The theory for heteronuclear decoupling is relatively straightforward when considering an isolated two-spin case, such as ^{13}C–^1H, and essentially perfect decoupling of the heteronuclear interaction is readily achieved (Waugh 1982). However, when the ^1H has a substantial J_{HH} coupling with a second proton, obtaining well-decoupled ^{13}C spectra becomes considerably more challenging (Barker et al. 1985). Qualitatively, this can be understood by considering that the ^1H irradiation largely removes the Zeeman part of the Hamiltonian, effectively creating a state where the two protons become strongly coupled, and approaching the condition of isotropic mixing (Braunschweiler and Ernst 1983; Barker et al. 1985). This so-called three-spin effect then can result in incomplete ^1H decoupling and a residual asymmetric splitting of the ^{13}C resonance (Shaka et al. 1987), and provided the impetus for the development of the DIPSI-type decoupling and isotropic mixing schemes (Shaka et al. 1988). The case of homonuclear $^{13}C'$–$\{^{13}C^\alpha, ^{13}C^\beta\}$ decoupling can actually be more demanding than for ^{13}C–$\{^1H^A, ^1H^B\}$ because the $^1J_{C\alpha C\beta}$ coupling is considerably larger than typical J_{HH} values, and the chemical shift differences between $^{13}C^\alpha$ and $^{13}C^\beta$ can be small, in particular for Ser and Thr residues. For this reason, the removal of three-spin effects can be more difficult at low field, and quite sensitive to the shape and duration of the $^{13}C^\alpha$ decoupling pulses as well as the interpulse delay, 2T. However, as demonstrated above and in Supplementary Fig. S1, good performance can be achieved with the single parameter set described here, over the entire range of commonly used magnetic field strengths in protein NMR, even though modest variations of these parameters can result in pronounced 3-spin effects (Supplementary Fig. S3).

Comparison of the intensities of the IPAP and LOW-BASHD versions of the 2D NCO spectrum of GB3 (Fig. 3B) indicates that, on average, LOW-BASHD offers an increase in S/N ratio of ca 35 % over IPAP, when using identical measurement times. For several residues, a somewhat larger gain is obtained. Inspection of these latter correlations reveals that in all cases they correspond to residues with small, nearly resolved long-range J_{CC} couplings to aliphatic side-chain carbons, that are largely decoupled by LOW-BASHD, but remain intact in the IPAP NCO spectrum. Lower enhancements are seen for correlations to Gly-$^{13}C'$ (red data points in Fig. 3B), owing to the larger offset of the Gly-$^{13}C^\alpha$ from the 59 ppm center of $^{13}C^\alpha$ decoupling, but also to the fact that in the IPAP-NCO spectrum these resonances are, on average, somewhat

narrower than for other residues due to the fewer long-range ^{13}C–^{13}C couplings.

As an application of the LOW-BASHD NCO experiment, and to illustrate that the resulting NCO spectrum permits quantitative analysis of its peak intensities, we use it to probe the intensity attenuation in the intrinsically disordered protein α-synuclein caused by the presence of small unilamellar phospholipid vesicles (SUVs). Prior work has shown strong attenuation of ^1H–^{15}N HSQC intensities of the N-terminal residues, without causing significant line-broadening (Eliezer et al. 2001; Bodner et al. 2009; Fusco et al. 2014). This attenuation has been attributed to a slow exchange process between the free state and multiple distinct lipid-interacting "dark states" (Bodner et al. 2009). A full understanding of the relaxation mechanism causing this dark state remains lacking, however.

The intensities observed in the LOW-BASHD NCO spectrum show a monotonically increasing attenuation of peak intensities when moving toward the N-terminus (Fig. 4). The smoothness of the attenuation pattern testifies to the accuracy of peak heights in the LOW-BASHD decoupled spectrum, even with these intensities spanning a 30-fold range in the lipid-containing sample.

The intensity attenuation pattern in the presence of SUVs is qualitatively very similar to that seen in the corresponding ^1H–^{15}N HSQC spectrum, except that the NCO spectrum shows stronger attenuation (Fig. 4B). This observation therefore rules out the possibilities that hydrogen exchange or paramagnetic contamination significantly impact this dark state relaxation process as these two processes would most attenuate the ^1H–^{15}N HSQC spectrum. The stronger attenuation seen towards the N-terminus in the 2D NCO intensities upon addition of lipid vesicles is caused by a small increase in transverse relaxation time noted previously and attributed to the k_{on} rate of protein residues binding to vesicles (Bodner et al. 2009). The effect is accentuated in the NCO relative to the HSQC spectrum due to the considerably longer $^1J_{NC'}$ de- and rephasing period (2×30 ms) compared to the $1/(2^1J_{NH})$ delays (2×5.3 ms) in the INEPT periods of the ^1H–^{15}N HSQC experiment. The attenuation profile is consistent with multiple distinct lipid binding modes of the protein: a ca 40 % fraction where residues 1–100 are lipid-bound and NMR invisible, and several other modes where a shorter N-terminal region is binding lipids, further attenuating the intensity of the remaining ∼60 % fraction. As previously pointed out (Bodner et al. 2009), the exchange rates for these less complete binding modes increase when involving shorter N-terminal fractions of the protein, increasing the effect of k_{on} on the transverse relaxation rates. This increased relaxation rate is responsible for the larger fractional attenuation in the NCO
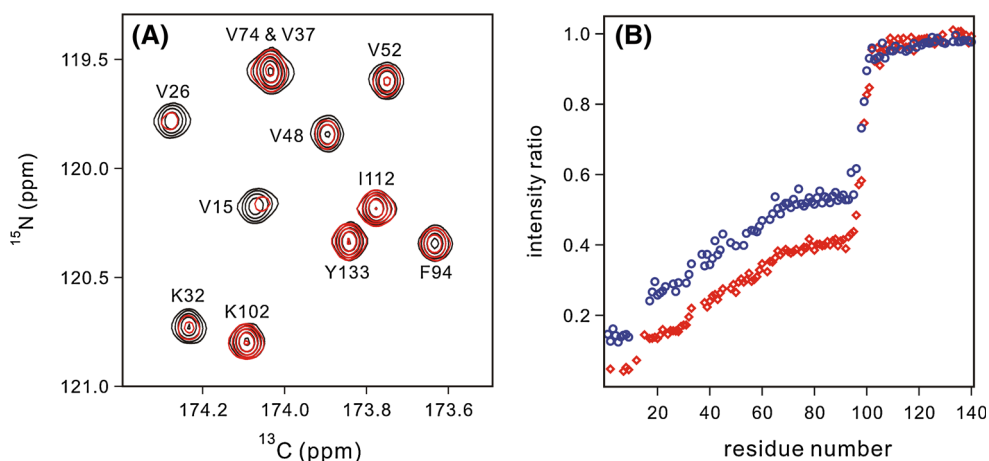
Fig. 4 Lipid-binding-induced intensity attenuation in the spectrum of uniformly ^{13}C/^{15}N-enriched, N-terminally acetylated α-synuclein, recorded at 800 MHz ^{1}H frequency. **A** 2D LOW-BASHD CON spectrum of 0.5 mM α-synuclein, 50 mM NaCl, pH 6.0, 288 K, in the absence (*black contours*) and presence (*red contours*) of 0.1 % small unilamellar vesicles (SUVs) consisting of a mixture of DOPE, DOPS and DOPC (in a 50:30:20 w/w/w ratio) used previously to mimic synaptic vesicles (Bodner et al. 2009). Correlations are labeled by the residue on which the ^{15}N resides. **B** The CON intensity ratio as a function of residue of spectra recorded in the presence and absence of SUVs (*red diamonds*) is shown together with the corresponding intensity ratios observed in the ^{1}H–^{15}N HSQC spectrum (*blue circles*). Corresponding peak volumes, which have somewhat larger statistical uncertainties, are compared in Supplementary Material Fig. S4. The time domain matrix for the CON spectrum consisted of 350 × 640 complex data points, or acquisition times of 134 ms (^{15}N) and 205 ms (^{13}C′), and of 512 × 1,024 complex data points, or acquisition times of 253 ms (^{15}N) and 102 ms (^{1}H) for the HSQC spectrum, with cosine bell apodization and doubling the length of all time domains by zero filling prior to Fourier transformation

relative to the HSQC spectrum of the most N-terminal residues. Note that, with the possible exception of the V15–G14 correlation, the attenuated resonances show no detectable change in frequency, despite the very high resolution of the spectrum.

Considering the relatively rapid translational diffusion observed for C-terminal residues of α-synuclein (Bodner et al. 2009), which retain nearly full intensity in the ^{1}H–^{15}N HSQC spectrum, our data strongly point to the presence of multiple distinct, long lived and relatively compact molten globule lipid-bound states, each subject to intermediate conformational exchange processes. Thus, under the NMR sample conditions used, the lipids are no longer part of the unilamellar vesicles added to the protein solution, but have been remodeled by the presence of α-synuclein.

In summary, we have shown that ^{13}C$^\alpha$ decoupling of ^{13}C′-observe experiments on uniformly ^{13}C-enriched proteins is readily possible, and can offer an advantage in terms of signal to noise over the popular IPAP method. The inverse application, where ^{13}C$^\alpha$ nuclei are directly observed and ^{13}C′ is decoupled, is also readily feasible by simply shifting the carrier frequency to ^{13}C$^\alpha$. This mode of decoupling is actually much less demanding, as the spectral width covered by ^{13}C′ is much narrower than for ^{13}C$^\alpha$, and three-spin effects are negligible because the ^{13}C′ is subject to only a single $^1J_{CC}$ coupling.

References

Barbet-Massin E, Pell AJ, Knight MJ, Webber AL, Felli IC, Pierattelli R, Emsley L, Lesage A, Pintacuda G (2013) 13C-detected through-bond correlation experiments for protein resonance assignment by ultra-fast MAS solid-state NMR. ChemPhysChem 14:3131–3137

Barker PB, Shaka AJ, Freeman R (1985) Homonuclear Hartmann–Hahn effects in broad-band decoupling. J Magn Reson 65:535–539

Bax A (1983) Broad-band homonuclear decoupling in heteronuclear shift correlation NMR spectroscopy. J Magn Reson 53:517–520

Bax A, Freeman R (1981) Investigation of complex networks of spin–spin coupling by two-dimensional NMR. J Magn Reson 44:542–561

Bax A, Mehlkopf AF, Smidt J (1979) Homonuclear broad-band decoupled absorption spectra. J Magn Reson 35:167–169

Bermel W, Bertini I, Felli IC, Kummerle R, Pierattelli R (2003) C-13 direct detection experiments on the paramagnetic oxidized monomeric copper, zinc superoxide dismutase. J Am Chem Soc 125:16423–16429

Bermel W, Bertini I, Duma L, Felli IC, Emsley L, Pierattelli R, Vasos PR (2005) Complete assignment of heteronuclear protein resonances by protonless NMR spectroscopy. Angew Chem-Int Ed 44:3089–3092

Bermel W, Bertini I, Felli IC, Piccioli M, Pierattelli R (2006) C-13-detected protonless NMR spectroscopy of proteins in solution. Prog Nucl Magn Reson Spectrosc 48:25–45

Bermel W, Bertini I, Chill J, Felli IC, Haba N, Kumar VMV, Pierattelli R (2012) Exclusively heteronuclear C-13-detected amino-acid-selective NMR experiments for the study of intrinsically disordered proteins (IDPs). ChemBioChem 13:2425–2432

Bodner CR, Dobson CM, Bax A (2009) Multiple tight phospholipid-binding modes of alpha-synuclein revealed by solution NMR spectroscopy. J Mol Biol 390:775–790

Braunschweiler L, Ernst RR (1983) Coherence transfer by isotropic mixing: application to proton correlation spectroscopy. J Magn Reson 53:521–528

Cavanagh J, Fairbrother WJ, Palmer AG, Rance M, Skelton N (2007) Protein NMR spectroscopy: principles and practice. MA, Elsevier Academic Press, Burlington

Delaglio F, Grzesiek S, Vuister GW, Zhu G, Pfeifer J, Bax A (1995) NMRpipe—a multidimensional spectral processing system based on Unix pipes. J Biomol NMR 6:277–293

Delsuc MA, Levy GC (1988) The application of maximum-entropy processing to the deconvolution of coupling patterns in NMR. J Magn Reson 76:306–315

Eletsky A, Moreira O, Kovacs H, Pervushin K (2003) A novel strategy for the assignment of side-chain resonances in completely deuterated large proteins using C-13 spectroscopy. J Biomol NMR 26:167–179

Eliezer D, Kutluay E, Bussell R, Browne G (2001) Conformational properties of alpha-synuclein in its free and lipid-associated states. J Mol Biol 307:1061–1073

Felli IC, Pierattelli R (2014) Novel methods based on C-13 detection to study intrinsically disordered proteins. J Magn Reson 241:115–125

Fusco G, De Simone A, Gopinath T, Vostrikov V, Vendruscolo M, Dobson CM, Veglia G (2014) Direct observation of the three regions in alpha-synuclein that determine its membrane-bound behaviour. Nat commun 5:3827

Garbow JR, Weitekamp DP, Pines A (1982) Bilinear rotation decoupling of homonuclear scalar interactions. Chem Phys Lett 93:504–509

Gil S, Hosek T, Solyom Z, Kuemmerle R, Brutscher B, Pierattelli R, Felli IC (2013) NMR spectroscopic studies of intrinsically disordered proteins at near-physiological conditions. Angewandte Chemie-Int Ed 52:11808–11812

Hammarström A, Otting G (1994) Improved spectral resolution in 1H NMR spectroscopy by homonuclear semiselective shaped pulse decoupling during acquisition. J Am Chem Soc 116:8847–8848

Levitt MH, Freeman R, Frenkiel T (1982) Broad-band heteronuclear decoupling. J Magn Reson 47:328–330

McCoy MA, Mueller L (1992a) Non-resonant effects of frequency-selective pulses. J Magn Reson 99:18–36

McCoy MA, Mueller L (1992b) Selective shaped pulse decoupling in NMR—homonuclear 13C carbonyl decoupling. J Am Chem Soc 114:2108–2112

Meissner A, Duus JO, Sorensen OW (1997) Spin-state-selective excitation. Application for E.COSY-type measurement of J(HH) coupling constants. J Magn Reson 128:92–97

Meyer NH, Zangger K (2013) Simplifying proton NMR spectra by instant homonuclear broadband decoupling. Angew Chem Int Ed 52:7143–7146

Nilsson M, Morris GA (2007) Pure shift proton DOSY: diffusion-ordered H-1 spectra without multiplet structure. Chem Commun 9:933–935

Sakhaii P, Haase B, Bermel W, Kerssebaum R, Wagner GE, Zangger K (2013) Broadband homodecoupled NMR spectroscopy with enhanced sensitivity. J Magn Reson 233:92–95

Shaka AJ, Barker PB, Freeman R (1987) 3-Spin effects in broad-band decoupling. J Magn Reson 71:520–531

Shaka AJ, Lee CJ, Pines A (1988) Iterative schemes for bilinear operators; application to spin decoupling. J Magn Reson 77:274–293

Struppe JO, Yang C, Wang YC, Hernandez RV, Shamansky LM, Mueller LJ (2013) Long-observation-window band-selective homonuclear decoupling: increased sensitivity and resolution in solid-state NMR spectroscopy of proteins. J Magn Reson 236:89–94

van de Ven FJM, Philippens MEP (1992) Optimization of constant-time evolution in multidimensional NMR experiments. J Magn Reson 97:637–644

Vander Kooi CW, Kupce E, Zuiderweg ERP, Pellecchia M (1999) Line narrowing in spectra of proteins dissolved in a dilute liquid crystalline phase by band-selective adiabatic decoupling: application to H-1(N)-N-15 residual dipolar coupling measurements. J Biomol NMR 15:335–338

Vogeli B, Kovacs H, Pervushin K (2005) Simultaneous H-1- or H-2-, N-15- and multiple-band-selective C-13-decoupling during acquisition in C-13-detected experiments with proteins and oligonucleotides. J Biomol NMR 31:1–9

Vuister GW, Bax A (1992) Resolution enhancement and spectral editing of uniformly ^{13}C-enriched proteins by homonuclear broadband ^{13}C decoupling. J Magn Reson 98:428–435

Waugh JS (1982) Theory of broad-band spin decoupling. J Magn Reson 50:30–49

Ying J, Roche J, Bax A (2014) Homonuclear decoupling for enhancing resolution and sensitivity in NOE and RDC measurements of peptides and proteins. J Magn Reson 241:97–102

Zangger K, Sterk H (1997) Homonuclear broadband-decoupled NMR spectra. J Magn Reson 124:486–489